

THE EFFECT OF THERMAL CONDITIONS ON PROCESS DEFECTS IN ELECTRON BEAM DIRECTED ENERGY DEPOSITION

R. Aman¹, A. Kitt¹, Z. Corey¹, L. Mohr¹, D. Ruscitto², N. Iyer², B. Rosenberger³

¹ EWI, Buffalo, NY 14211 ² GE Global Research, ³ Lockheed Martin Corporation

Abstract

Observing process defects at size scales and with sufficient confidence relevant to qualification efforts has not yet been achieved in metal AM, so non-destructive testing (NDT) techniques are used to detect porosity within material deposited. NDT costs can be significant and may not achieve targeted resolution due to geometry and material limitations. In this work, in-process monitoring of Electron Beam Directed Energy Deposition (EB-DED) is enhanced to include three thermal history conditions; inter-pass, melt pool superheat and trailing bead temperatures. Quality scenarios are applied to simulate various process conditions during EB-DED at three different thermal conditions within production relevant use cases and resultant process defects are characterized via high throughput computed tomography. Defects are spatially and temporally registered to process conditions observed during EB-DED and statistically mapped to thermal scenarios. Thermal condition has a strong influence on the quantity of observed process defects, with lower interpass temperature resulting in a larger number of defects.

Introduction

Electron Beam Directed Energy Deposition (EB-DED) is a wire-based additive manufacturing (AM) process capable of high material deposition rates as high as 40 lbs/hr or more. Aerospace, nuclear and marine applications use EB-DED because of the low oxygen environment and the high weld quality that results. An example component produced using EB-DED technology is the titanium fuel tank dome for satellites (Sciaky, Inc., 2018). EB-DED has been demonstrated on a wide range of materials including nickel alloys (Matz 1999, Bird 2009, Hales 2020), aluminum (Tamingier 2002), titanium (Wallace 2004), stainless steel (Wanjara 2007) and other materials including gradient compositions (Brice 2014).

EB-DED systems generally consist of vacuum chambers (Figure 1), electron guns, motion and control systems. The EB-DED process is performed in a high vacuum environment (10^{-5} torr) and is capable of 3, 4 or 5 axis deposition by using Computer Numerical Control (CNC) programming. Due to operation in a vacuum, heat transfer out of the workpiece is primarily conduction and radiation modes and alloys containing elements with different vapor pressures will preferentially vaporize those with the higher vapor pressure. The resulting metal vapor deposits on cool surfaces within the vacuum chamber, including wire nozzles, antenna plates, chamber walls and other equipment.

Thermal energy is delivered in the form of a stream of electrons originating at a thermionic emitter and accelerated by electrostatic potential (accelerating voltage) between a cathode and an anode in the electron gun. This stream of electrons passes through focusing coils and deflection coils which control the beam energy distribution at the deposition plane. The accelerating voltage and beam current (BC) can be used to control the total energy applied, and beam focus and deflection can be used to control the distribution of the energy.

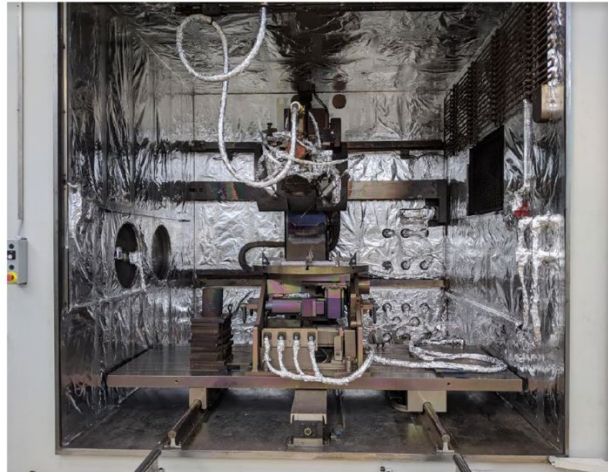


Figure 1. Sciaky EBAM/EBW VX.3-110x110x110 EB-DED vacuum chamber at EWI.

A closed loop control (CLC) system uses a visible light camera to observe the weld pool and adjust BC to maintain a consistent weld bead width. The bead width set point (BWS) can be adjusted dynamically in the CNC program to compensate for regions of the part which have less or more physical material support (e.g. thin walls or thick sections).

Defects specific to EB-DED have not been well characterized in the literature, but may be considered similar to those observed in other wire-based DED processes (Liu, 2021). Internal defects such as lack of fusion (LOF) and porosity are a primary concern due to the impact these defects have on mechanical properties and service life (Liu Z. K., 2019). Geometric defects, e.g. distortion due to thermal stress, may cause interference of the part with the deposition systems during the AM process (Stecker 2015) and in extreme instances result system crashes. Compositional defects may arise out of metal vapor deposits dislodging from the antenna plate or wire nozzles and landing on the surface or directly in the weld pool.

The direct observation of LOF and porosity defects during the deposition process can be challenging if the defect is small or if obstructed from sensor view by material. Nondestructive evaluation (NDE) methods such as ultrasonic testing (UT) or computed tomography (CT) can be used in some cases to verify part quality, but AM materials can be difficult to assess due to directional solidification microstructure and the part size or physical accessibility (Freed, 2017). Therefore, in-process monitoring is often used to identify conditions that may result in defects.

The influence of thermal conditions on defect manifestation is not well studied in EB-DED. Thermal conditions can change based on geometry and process flow. Components made via EB-DED may have thin wall sections made up of a single bead width or large multi-bead thick sections. Process flow may be impacted by the need to stop production to perform maintenance or operator shift changes, or the need for an intermediate stress relief operation before continuing on large components.

Component production via EB-DED has been demonstrated to be cost effective for a target *drop link* aerospace component, but inspection costs eliminate the advantage. Inspection costs can be reduced by 1) improving confidence in process signals indicating the likelihood of defects during production and 2) utilizing a criticality zoning of the component for thresholding the impact of potential defects. The purpose of this study is to understand the role of thermal conditions, particularly interpass temperature, on defect manifestations to inform the need for preheating or establishing limits on inter-pass temperatures based specifically on defect likelihood.

Materials and Methods

A Sciaky EBAM/EBW VX.3-110x110x110 EB-DED system (S/N 11756) with CLC was outfitted with a Micro-Epsilon TIM640 thermal camera, a Micro Epsilon CTL40 pyrometer and a ratio pyrometer to observe weld bead temperature, inter-pass temperature and melt pool temperature respectively. A metal vapor protection system with a polyimide film was implemented to protect the TIM640 and CTL40. The CLC camera system has a small helium gas purge which was modified to also protect the ratio pyrometer optical train. Signals from these instruments were collected on a separate data computer.

Production relevant Ti-7Al-4V wire (Perryman Company, Houston, PA) with 1/8-in. diameter was used. Chemistry was modified from typical titanium alloy grade 5 to account for preferential vaporization of aluminum.

The IR instruments were calibrated using EB-DED deposited Ti-7Al-4V in bead form with a reference thermocouple mounted to the bottom. The calibration coupon was thermally isolated and electrically connected to the machine frame and calibration was performed with the electron beam heating the coupon top surface. A five-step thermal calibration was performed and linear regression applied to the resulting data. Intrinsic and extrinsic calibrations for IR instruments were performed via an internal procedure.

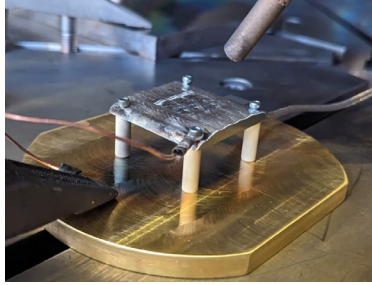


Figure 2. Thermal calibration coupon produced using EB-DED process and machined to minimize thermal mass. Coupon is thermally isolated from base via ceramic stand-offs and electrically connected via copper wire. Thermocouple is mounted to the bottom of the calibration coupon.

The in-process monitoring data is collected on two different computers. The PLC computer collects machine position, machine logs and PLC camera images and the data monitoring computer collects TIM640 images, CTL40 interpass temperature and ratio pyrometer data. The two computers are temporally registered with a synchronization signal from the EB-DED controller. Combining the extrinsic calibration and temporal synchronization, thermal data can be spatially registered to machine position at any instance in time.

EB-DED parameters for 6.8 kg/hr Ti-7Al-4V deposition are based on those used in the production of the reference part (Table 1). Production relevant thermal conditions were validated by deposition of the reference part in the production configuration. Note that Ti-7Al-4V material is used to compensate for the vaporization of approximately 1wt% aluminum during the process.

Table 1. Production relevant EB-DED process parameters

Parameter	Nominal
Accelerating Voltage	40kV
Beam Current	235mA
Beam Focus	355mA (30 mA above sharp focus)
Spot Size	7.54mm
Travels Speed	750mm/min
Stepover	9.1mm
Layer Height	3.4mm
Dynamic Raster	On
Closed Loop Control	Off
Wire Feed Speed	3.2m/min
Bead Width Setpoint	11.9mm

Test blocks were designed targeting dimensions of 200x50x50mm, with a region of interest between 38 and 114mm from the start in the *x* direction (Figure 3). The size of the test block was limited to allow a target voxel size of 45 μ m in the rapid characterization micro-Computed Tomography (μ CT) equipment. This provided the ability to reliably detect 250 μ m defects in the Ti-6Al-4V test blocks.

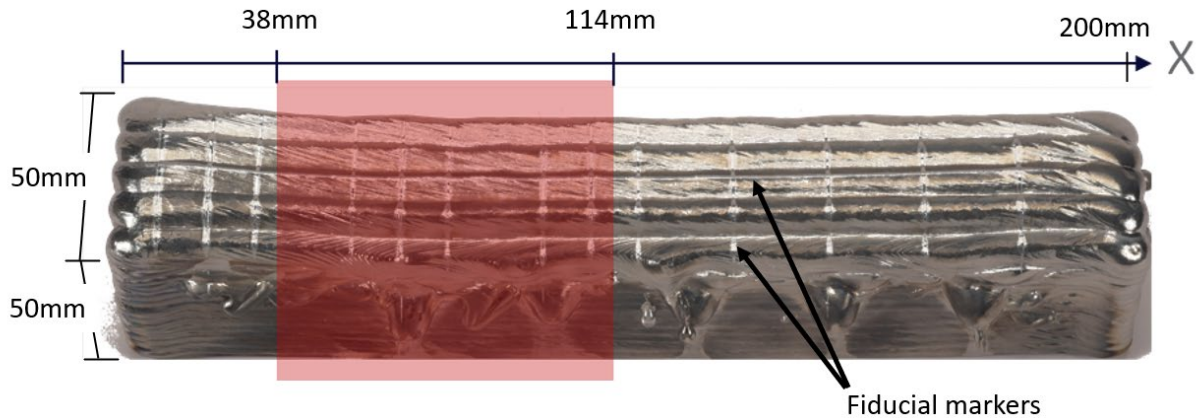


Figure 3. Test block configuration showing dimensions and fiducial markers for registering μ CT and deposition machine coordinate frames. Highlighted region indicates region of interest for quality scenarios and inspection.

Fiducial markers were added to each test block using a focused electron beam scan at low energy to indicate machine coordinate frame locations and to serialize the test coupons. Fiducial markers were located at 50.8, 76.2, and 101.6mm along the x direction and -18.3mm along the y direction for all test blocks and additional fiducial markers were added based on block serial number as necessary.

Quality Scenarios (QS) were established to introduce defects into the test blocks. Process experts and EB-DED end use stakeholders were interviewed to identify key process conditions which are likely to introduce LOF and porosity defects during production (Table 2). The QS were further developed to establish 25 test levels of 7 scenarios.

Table 2. QS identified by EB-DED process experts and stakeholders.

Scenario	Levels	Count
Power cycle in short period of time (keyhole)	0, 100%	2
Off-center wire relative to melt pool	0.030, 0.060, 0.075	3
Incorrect height of wire relative to weld pool	(+/-).09, 0.12, -0.15, +0.03, +0.06	7
Wire stop	0	1
Loss of deflection control	Off	1
Focus values	(+/-) 10, 20, 30 focus points (amps)	6
Scale Factor (XSF/YSF – spot size)	(+/-) 10, 25 and -50	5

Thermal conditions of a production component were observed during deposition (Figure 4) to establish thermal scenarios (TS) for the test blocks. The production test included a double-sided build of two components with test coupons using parameters outlined above (Table 1).

Deposition alternated build plate sides each layer to balance stresses as in the production of the actual component. Prior to deposition of each layer, inter-layer temperature was captured using the CTL40 pyrometer in the regions to be deposited. A histogram of observed inter-layer temperatures is provided in Figure 5.

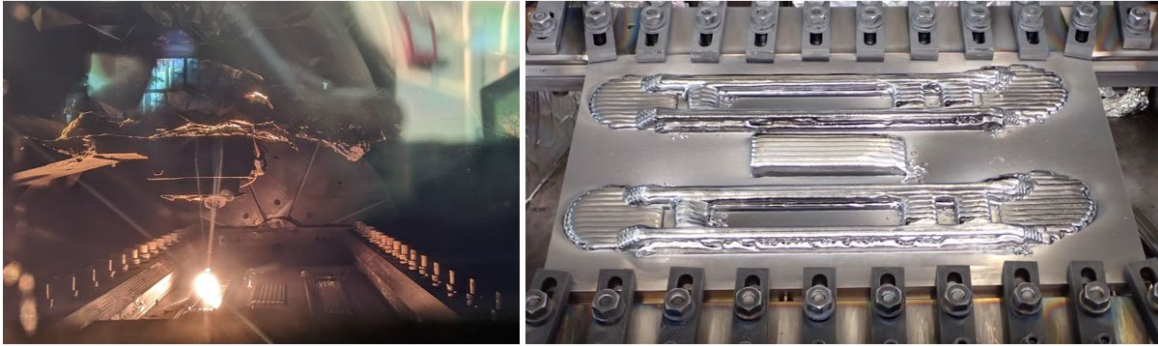


Figure 4. Test deposition of production component to establish upper bound for inter-pass temperature on TS during deposition (left) and resulting deposition (right).

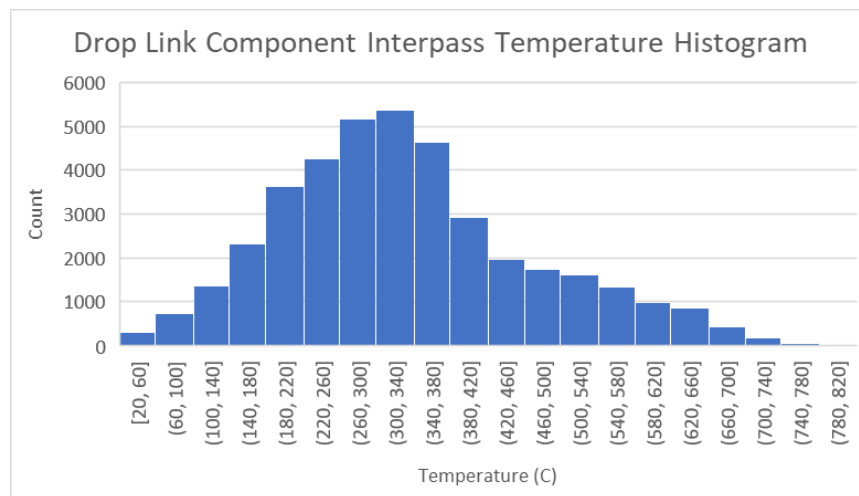


Figure 5. Observed inter-layer temperatures from production component.

Five test blocks were produced with intentional defect conditions, each with five QS and three TS. Test blocks were 5 beads wide and 15 layers tall. Each layer was assigned a single QS and the 5 QS per test block were repeated three times, once for each TS. Three different inter-layer dwell times (60, 30 and 15 seconds) were used to establish the different TS. Two additional test blocks were produced, one with nominal production conditions and a second with conditions that will not be considered in this work.

Test blocks were laser scanned, removed from the substrate via bandsaw, and μ CT scanned. All μ CT measurements were acquired at GE Global Research (Schenectady, NY) using a Phoenix VtomeX 300M dual tube instrument with scan parameters optimized using scrap EB-DED Ti-6Al-4V material. The test blocks were positioned in the instrument with the long axis oriented vertically, permitting the required 360-degree rotation for data acquisition and volume

reconstruction. One-thousand images were collected as the sample was rotated under irradiation from the microfocus tube (240 kV, 160 μ A) using a 2024 x 2024 pixel GE DXR250RT Xray detector. The field of view for the images was approximately 89mm down the length of the test block and total scan time was \sim 34 minutes. The images were reconstructed into a 3D volume using Phoenix Datas (v2.3.0) software. The reconstructed dataset was imported into VGStudio MAX 3.0 and then manipulated to orient the volume and exported as a stack of 8-bit images (tiffs) oriented down the long axis of the sample for subsequent viewing and processing in ImageJ/FIJI (Schindelin, 2012) and AVIZO3D¹ (Figure 6). Final pixel resolution for the reconstructed datasets correspond to 45 μ m; suitable to resolve minimum detectable features of 250 μ m diameter.

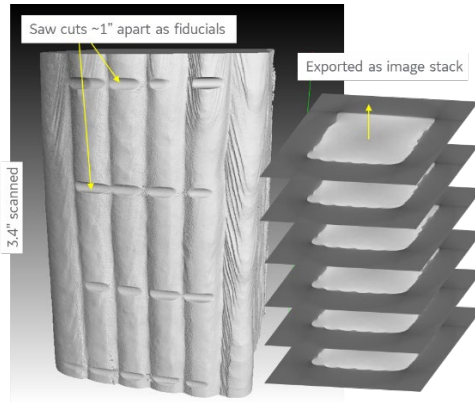


Figure 6. Annotated 3D reconstruction of Ti-6Al-4V setup block.

Defect spatial registration was established by performing a best fit alignment of the fiducial features produced during deposition (Figure 7). Defects were then labeled with the machine coordinate frame values for attributing to specific beads and layers.

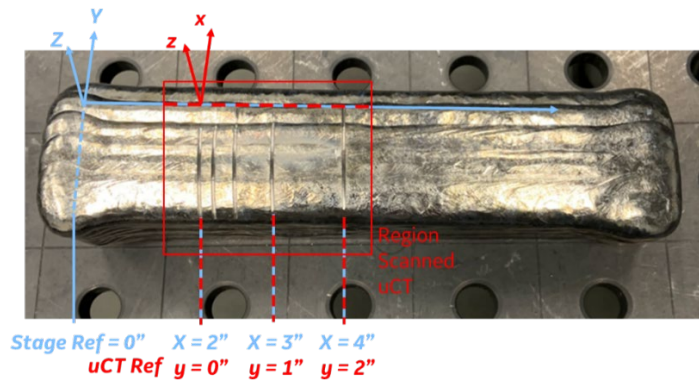


Figure 7. Test block registration of μ CT scan coordinate frame (red) to machine coordinate frame (blue) using fiducial markers.

Results

¹ AVIZO3D 2022.1 is a commercial software package produced by Thermo Fisher Scientific

Defect count, size and shape are presented in Table 3. Attribution of defects to individual QS is beyond the scope of this paper. Two defects in test block Specimen 1 were found to be in close proximity to one another (distance between defects less than the size of the largest defect) and converted to a single defect. A total of 155 defects greater than 250 μ m were labeled across the 7 test block specimens.

Table 3. Defect count per block including size (Equivalent Spherical Diameter - ESD) and shape of defects statistics.

Specimen	# Indications	Mean ESD (μ m)	1 SD ESD (μ m)	Mean Shape Factor ¹	1SD Shape Factor
1	99*	496.7	317.4	3.66	3.99
2	22	403.4	203.2	2.36	1.52
3	3	273.3	50.1	1.24	0.38
4	22	504.4	290.3	2.78	2.03
5	1	301.8	-	1.09	-
6	5	306.0	154.7	2.09	0.61
7	3	486.8	291.0	1.15	0.19
Total	155*	472.8	293.5	3.19	3.40

¹ Shape factor = 1.00 is a perfect sphere, larger values represent less compact volumes

*Note: one pair of discontinuities was found to be within close proximity to one another and so converted to a single defect.

Defects were assigned to TS by considering the location based on the layer it was registered to (Table 4). Approximately 76% of all defects were from TS1 and 20% from TS3. The fewest defects were registered to TS2, at only 4%. Observed inter-pass temperatures per weld bead are shown in Figure 8.

Table 4. Defect allocation to TS vs. test block specimen.

Specimen	Defect count	Defect count		
		TS 1	TS 2	TS 3
1	99	80	3	16
2	22	17	2	3
3	3	1	1	1
4	22	16	0	6
5	1	0	0	1
6	5	1	0	4
7	3	3	0	0
Totals	155	118	6	31

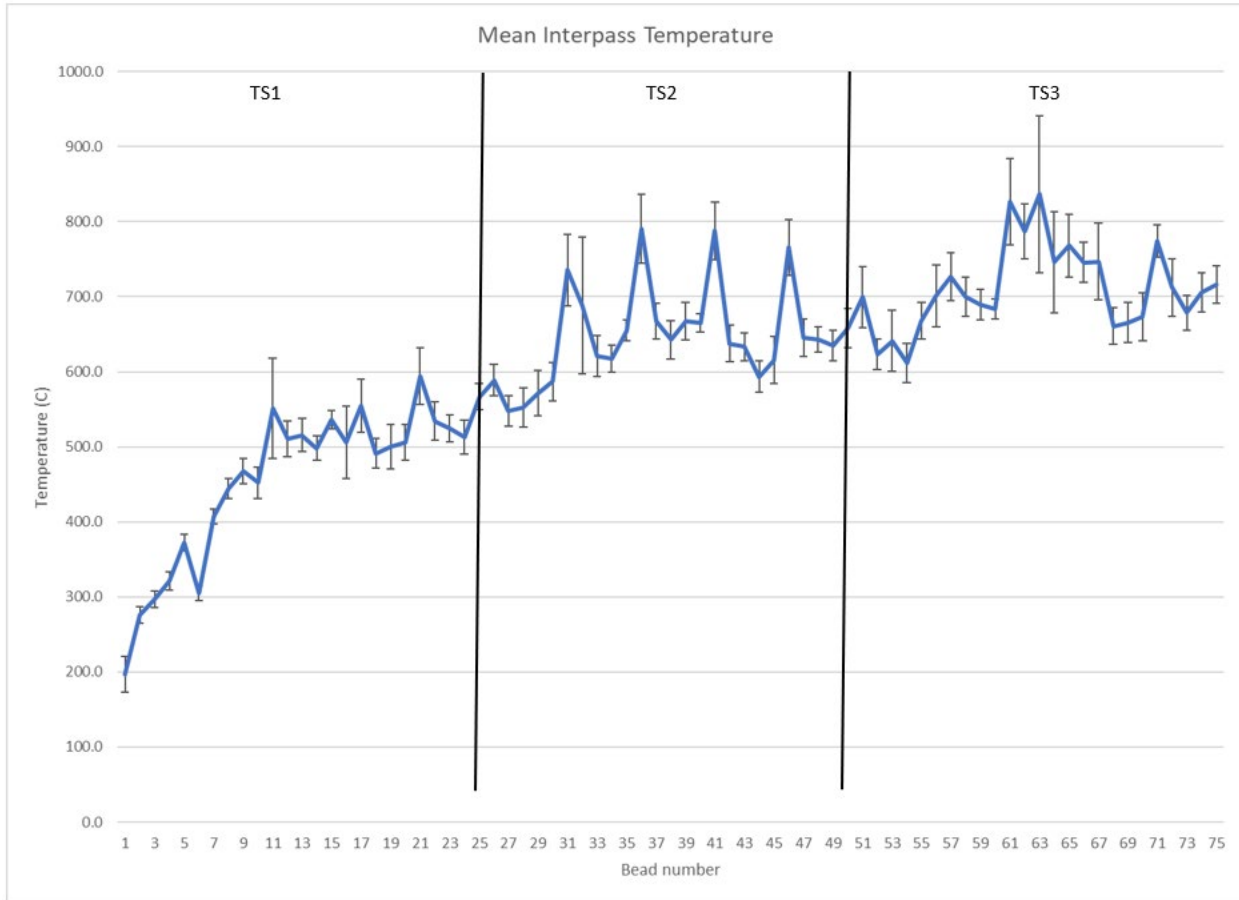


Figure 8. Observed inter-pass temperatures for weld beads (error bars are one standard deviation)

The average inter-pass temperatures for TS1 was 452°C with standard deviation (SD) of 102°C. Average inter-pass temperature for TS2 was 649°C and SD of 64°C. For TS3, average interpass temperature was 712°C and SD of 56°C.

Discussion

A majority (76%) of defects were observed in TS1 indicating that, for a given QS, defects are more likely at lower inter-pass temperatures. This is a novel observation in EB-DED processing and should be considered when developing production qualification schema.

The difference in defect concentrations is caused by the melt pool being closer to solidus temperature during processing. A rigorous estimate of temperature can be obtained based on changing parameters during heat (Rykalin, 1977), but simplification can be used in this case:

$$T_m = T_0 + \frac{Q}{cm} \quad (1)$$

Where T_m is an estimate of the melt pool temperature, T_0 is the interpass temperature, Q is heat input (EB-DED power), c is the specific heat capacity and m is the mass. Thus for a given power

and material condition, a lower interpass temperature will result in a lower melt pool temperature. Surface tension is temperature dependent in liquid metals and has been shown to influence Marangoni flow of molten metals (Egry, 2010). Therefore the influence of TS on defect manifestation can be attributed to the temperature difference and may be overcome with adjustments to input power to maintain T_m constant.

In this study, no preheat was applied to the base plate and the CLC was not in operation. If the CLC is placed in operation, the beam current is adjusted automatically to maintain the bead width at the bead width setpoint. In that case, it may be possible to reduce the likelihood of defects because the machine may compensate for the lower inter-pass temperature with higher beam current.

Interpass temperature rises quickly in the EB-DED process and dissipates very slowly due to the weak thermal coupling between the base plate and the machine foundation. In addition, convection heat transfer is very small due to the vacuum environment. Titanium alloy has a low heat transfer coefficient and the accumulated heat tends to remain in the weld region for a significant amount of time. In future studies, longer inter-layer delay time should be deployed to reduce the layer temperature standard deviation.

The observed interpass temperatures from the test block specimens were consistent with the inter-layer temperatures observed in the production test. Several inter-pass temperatures observed in beads in TS2 were higher relative to adjacent beads, and periodically consistent. Further investigation is ongoing to identify the cause of these temperature spikes.

Conclusion

Lower interpass temperatures has been shown to result in more defects in EB-DED under similar processing conditions. When process conditions lead to lower inter-pass temperatures (e.g. long process pauses for maintenance, operation schedule or stress relief) preheating should be considered to reduce the likelihood of defects. An alternative may include adjusting input power to maintain melt pool temperature constant.

Acknowledgements

This work is supported by the US Department of Energy office of Energy Efficiency under award DE-EE0009399.

References

- [Bird, 2009] Bird, R. K., & Hibberd, J. (2009). Tensile Properties and Microstructure of Inconel 718 Fabricated with Electron Beam Freeform Fabrication (EBF (sup 3)).
- [Brice 2014] Brice, C. A., Newman, J. A., Bird, R. K., Shenoy, R. N., Baughman, J. M., & Gupta, V. K. (2014). *Electron beam freeform fabrication of titanium alloy gradient structures*. National Aeronautics and Space Administration, Langley Research Center.
- [Egry 2010] Egry, I. R. (2010). Surface tension of liquid metals and alloys—Recent developments. *Advances in colloid and interface science*, 198-212.

- [Freed 2017] Freed, S. T. (2017). *Nondestructive Post-process Evaluation of Additively Manufactured (AM) Parts*. Columbus: Additive Manufacturing Consortium.
- [Hales 2020] Hales, S. J., Domack, C. S., & Taminger, K. M. (2020). Electron Beam Freeform Fabrication of Dissimilar Materials: Cracking in Inconel® 625 Deposited on GRCo-84. TP-2020-5005040, NASA, <https://ntrs.nasa.gov/api/citations/20205005040/downloads/NASA-TP-2020-5005040.pdf>
- [Liu 2021] Liu, M. K. (2021). A Review of the Anomalies in Directed Energy Deposition (DED) Processes & Potential Solutions - Part Quality & Defects. *NAMRC49* (pp. 507-518). Cincinnati: Elsevier B.V.
- [Liu 2019] Liu, Z. K. (2019). Influence of energy density on macro/micro structures and mechanical properties of as-deposited Inconel 718 parts fabricated by laser engineered net shaping. *Journal of manufacturing processes*, 96-105.
- [Matz 1999] Matz, J. E. (1999). *Carbide formation in a nickel-based superalloy during electron beam solid freeform fabrication* (Doctoral dissertation, Massachusetts Institute of Technology).
- [Rykalin 1977] Rykalin, N. N. (1977). Calculation of the heating of materials by laser radiation allowing for the temperature dependences of thermal properties. *Soviet journal of quantum electronics*, 853.
- [Schindelin 2012] Schindelin, J. A.-C.-Y. (2012). Fiji: an open-source platform for biological-image analysis. *Nature Methods*, 676-682. doi:doi:10.1038/nmeth.2019
- [Sciaky 2018] Sciaky, Inc. (2018, July 18). *News and Events: Press Releases - Sciaky's Electron Beam Additive Manufacturing (EBAM®) Process Achieves Qualification for Huge Satellite Fuel Tanks*. Retrieved from Sciaky.com: <https://www.sciaky.com/news/press-releases/sciaky-s-electron-beam-additive-manufacturing-ebam-process-achieves-qualification-for-huge-satellite-fuel-tanks>
- [Stecker 2015] Stecker, S.D., Lachenberg, K., Panano, M., Mugnaini, A. (2015). Large Melt Pool Electron Beam Additive Manufacturing of Titanium. In *SAMPE Baltimore Conference and Exhibition 2015*. Society for the Advancement of Material and Process Engineering.
- [Taminger 2002] Taminger, K., & Hafley, R. A. (2002). Characterization of 2319 aluminum produced by electron beam freeform fabrication. In *2002 International Solid Freeform Fabrication Symposium*.
- [Wallace 2004] Wallace, T. A., Bey, K. S., Taminger, K., & Hafley, R. A. (2004). A design of experiments approach defining the relationships between processing and microstructure for Ti-6Al-4V. In *2004 International Solid Freeform Fabrication Symposium*.
- [Wanjara 2007] Wanjara, P., Brochu, M., & Jahazi, M. (2007). Electron beam freeforming of stainless steel using solid wire feed. *Materials & design*, 28(8), 2278-2286.